A new flexible reconstruction framework for motion correction in SPECT imaging

Hanno Schumacher, Bernd Fischer

Abstract—**Due to the long imaging times in SPECT, patient motion is inevitable and constitutes a serious problem for any reconstruction algorithm. The measured inconsistent projection data lead to reconstruction artifacts which can significantly affect the diagnostic accuracy of SPECT if not corrected. Among the most promising attempts for addressing this cause of artifacts is the so-called data-driven motion correction methodology, implemented, for example, in the OSEM scheme. At present, this algorithm is restricted to the exclusive use of a dual-head SPECT system with perpendicular heads and incorporating in a subset only projection data obtained between a patient movement. The utilization within other SPECT systems may lead to unsatisfactory results. In this note we present a new reconstruction framework which overcomes these two shortcomings. Within the new framework, the user may choose any set of projection for the reconstruction and the scheme works for any SPECT system. As a byproduct, the well-known EM and OSEM reconstruction schemes may be written in terms of the new framework and therefore are included in the theoretical considerations. The paper is supplemented by a large set of test examples, underscoring the potential power of the proposed novel approach. Using both an academic example and images from a double-head detector we studied the extent of defects induced by simulated motion and validated the new schemes.**

Index Terms—**reconstruction algorithm, data-driven motion correction, SPECT**

I. INTRODUCTION

IN Single Photon Emission Computed Tomography (SPECT), the imaging time is typically in the range of 5-30 minutes. Here, patient movement, which has frequently been reported in clinical applications [1], constitutes a serious problem for any reconstruction scheme. The movements cause misalignment of the projection frames, which degrades the reconstructed image and may introduce artifacts. These motion artifacts may significantly affect the diagnostic accuracy [2]–[4]. Different methods have been proposed for the correction of motion in SPECT studies. These methods may be divided into three categories. The first two approaches do produce motion corrected projections and thus may be used in conjunction with any reconstruction method. The first approach is purely hardware based, like, for example the triple scan [5] or dual scan [6] protocol. The second approach corrects for the patient motion by using a computational method applied within the projection-space [7]–[9]. It should be noted, that due to the projection geometry the latter method is not able to compensate for rotational movement. In this paper, we are concerned with the third methodology. Here the correction is performed in the image space. A widely used member out of this class is the so-called data driven motion correction

H. Schumacher and B. Fischer are with the Institute of Mathematics, University of Lübeck, Wallstrasse 40, 23554 Lübeck, Germany.

(DDMC) approach [10], [11]. It can handle full 3D rigid-body motion (6 degrees of freedom) that occurs between projections. For an approach used in reconstruction of PET images, including motion correction in a single projection see [12] and references therein. To start the scheme, it is assumed that the rigid-body motion of the patient is known. The actual determination of the movement is not subject of this paper, see [11], [13], for an overview in this direction. Once the motion is known it needs to be corrected. The idea is to subdivide the projection data into subsets where no motion has been detected and to move the object estimate for each of these subsets accordingly. To this end the rigid-body parameters after the ith movement of the patient are stored in the vector S_i. Furthermore, all projections that were measured between the ith and the $i+1$st movement are collected in the projection set $\mathbf{P}_i$. The image, which has been in the course of the algorithm reconstructed up to the ith step, is denoted by $\mathbf{f}^{(i)}$. This image has to be corrected with respect to the next object position S_{i+1}. The result is denoted by $\mathbf{f}^{(i)}(S_{i+1})$. Next the partial reconstruction $\mathbf{f}^{(i)}(S_{i+1})$ is updated with the help of measured projections $\mathbf{P}_{i+1}$ via

$$\mathbf{f}^{(i+1)} = \mathbf{R}[\mathbf{P}_{i+1}, \mathbf{f}^{(i)}(S_{i+1})], \tag{1}$$

where $\mathbf{R}$ denotes a reconstruction algorithm. Ideally, the resulting image $\mathbf{f}^{(m)}$ should contain less motion artifacts. An important ingredient in the overall scheme is an interpolation method taking care of the necessary image interpolation in the m steps of the scheme, in particular for the computation of $\mathbf{f}^{(i)}(S_{i+1})$. Here, we refer to [14] and references therein. A widely used reconstruction algorithm is the so-called OSEM algorithm [15]. It employs iteratively projection and backprojection in order to calculate a reconstruction based on the actual set of projections. As we are working with discrete data, the projection and backprojection needed in the OSEM scheme may be written in terms of matrices $\mathbf{A}$ and $\mathbf{A}^\top$, respectively. $\mathbf{A}$ is frequently called the probability density matrix (PDM). Let $\mathbf{A}_{i+1}$ denote the projection matrix corresponding to the projection set $\mathbf{P}_{i+1}$. The update scheme (1) together with the OSEM algorithm may then be conveniently written as

$$\mathbf{f}^{(i+1)} = \mathbf{f}^{(i)}(S_{i+1}) \cdot \left(\frac{\mathbf{A}_{i+1}^\top \left(\frac{\mathbf{P}_{i+1}}{\mathbf{A}_{i+1}\mathbf{f}^{(i)}(S_{i+1})} \right)}{\mathbf{A}_{i+1}^\top \mathbf{1}} \right). \tag{2}$$

Here $\mathbf{1} = (1, \ldots, 1)^\top$ denotes a vector corresponding to the size of $\mathbf{A}_{i+1}^\top$. Furthermore, the notation $\mathbf{x} \cdot \mathbf{y}$ and $\frac{\mathbf{x}}{\mathbf{y}}$ indicates a component wise multiplication and division of the vectors $\mathbf{x}, \mathbf{y}$. For convenience, we assume throughout the paper that the denominator has no zero components.

As it is apparent from the update scheme (1), the projection sets to be processed in the OSEM reconstruction scheme are bounded to be a subset of $\mathbf{P}_i$. Due to the fact that this scheme is restricted to dual-head SPECTs with perpendicular sensors the subsets will always contain projections measured at perpendicular angles. It is this choice which may lead to unsatisfactory results for other SPECT systems. It is the goal of this paper to provide a theoretical framework which does allow for any choice and enumeration of projections. As it turns out, all reconstruction algorithms using projection/backprojection methodology may be phrased in terms of the new framework. This in particular includes the well-known EM [16], [17], OSEM [15], and HOSP [18] scheme (see [19] for further examples). However, as we will indicate in the next section, one may as well design completely new schemes. In addition, based on the theoretical framework it is possible to come up with a sound convergence proof for some of the schemes belonging to the above mentioned class. We will report on convergence results in a forthcoming paper.

II. THE NEW FRAMEWORK

The idea is to view the DDMC reconstruction scheme as a least-squares approximation problem

$$\frac{1}{2}\|\hat{\mathbf{A}}\mathbf{f} - \mathbf{g}\|_2^2 \rightarrow \min, \tag{3}$$

where $\hat{\mathbf{A}}$ is a matrix which has at least as many rows as columns, $\mathbf{f}$ and $\mathbf{g}$ are vectors of appropriate size, and $\|.\|_2$ denote the Euclidean vector norm. It is well known that a solution for (3) is characterized by the normal equation (see, e.g. [20])

$$\mathbf{0} = \hat{\mathbf{A}}^\top(\hat{\mathbf{A}}\mathbf{f} - \mathbf{g}) = \hat{\mathbf{A}}^\top\left(\mathbf{1} - \frac{\mathbf{g}}{\hat{\mathbf{A}}\mathbf{f}}\right) \cdot \hat{\mathbf{A}}\mathbf{f}.$$

Assuming that $\hat{\mathbf{A}}\mathbf{f}$ and $\hat{\mathbf{A}}^\top\mathbf{1}$ have no zero components, we deduce

$$\mathbf{0} = \mathbf{f} \cdot \hat{\mathbf{A}}^\top(\mathbf{1} - \frac{\mathbf{g}}{\hat{\mathbf{A}}\mathbf{f}}) = \mathbf{f} \cdot \left(\mathbf{1} - \frac{\hat{\mathbf{A}}^\top\left(\frac{\mathbf{g}}{\hat{\mathbf{A}}\mathbf{f}}\right)}{\hat{\mathbf{A}}^\top\mathbf{1}}\right) \cdot \hat{\mathbf{A}}^\top\mathbf{1},$$

which in turn leads to the wanted representation of a solution of (3)

$$\mathbf{f} = \mathbf{f} \cdot \left(\frac{\hat{\mathbf{A}}^\top\left(\frac{\mathbf{g}}{\hat{\mathbf{A}}\mathbf{f}}\right)}{\hat{\mathbf{A}}^\top\mathbf{1}}\right). \tag{4}$$

Note that this representation has the same structure as the one for the OSEM algorithm (2). The essential difference is the fact that the right hand side of the OSEM update depends on $\mathbf{P}_{i+1}$ and S_{i+1}, i.e. it changes for each iteration step. To turn (4) into a useful update formula for a projection/backprojection based motion correction scheme, we simply choose

$$\hat{\mathbf{A}} = (\hat{\mathbf{A}}_1, \ldots, \hat{\mathbf{A}}_m)^\top \quad \text{and} \quad \mathbf{g} = (\mathbf{P}_1, \ldots, \mathbf{P}_m)^\top,$$

where $\hat{\mathbf{A}}_i = \mathbf{A}_i\hat{\mathbf{S}}_i$ and $\hat{\mathbf{S}}_i$ encodes the accumulated patient movement from the original position to the ith position.

Furthermore, $\mathbf{P}_i$ is a set of projections of the same motion state.

Note, that the framework is based on the assumption that the motion occurs between two projections. For the correction of motion that occurs inbetween two projections, we refer to [12], where the reconstruction of PET images is considered. It is worthwhile to note, that (4) looks like the well-known formulation of the EM algorithm. However, in its conventional implementation, the EM scheme does not include any motion information in its projection matrix $\hat{\mathbf{A}}$. In other words, the update formula (4) constitutes an EM algorithm with motion correction, which we will call EMMC. Along the same lines we may use (4) to formulate a variant OSEMMC of the OSEM algorithm with motion correction. Due to the fact that all motion information is included in the projection matrix $\hat{\mathbf{A}}$, the restriction to the motion-free projections, as in (2), is no longer necessary. This leaves the user with the problem on which projection sets are to be chosen and which are for which situation the best. For further information to this topic see [21]. However, in the result section we discuss one possible choice. Also, one may incorporate the motion correction facility in schemes other than EM and OSEM, like for example the HOSP scheme. Even if one designs a completely new scheme our framework can be included to perform a reconstruction with motion information as long as this scheme is using a projection/backprojection matrix.

III. RESULTS

In this section we report on some numerical test runs. To confirm the accuracy of the methods, we apply the EMMC, the original OSEM (see (2)), and the OSEMMC scheme to both 3D academic examples and 3D phantom experiments. The academic data simulate a one-head system whereas the latter data were produced by a two-head SPECT without perpendicular heads. Consequently the requirements for the OSEM algorithm using the DDMC scheme are violated. Nevertheless, we still applied the OSEM scheme for comparison purposes. For the same reasoning the EM algorithm without motion correction is applied. The implementations were purely done in MATLAB, therefore we do not report on execution times or memory requirements.

A. Academic example

We start out with a purely academic example. Here the object is a cylinder of size $64 \times 64 \times 64$ (see figure 1), which may be interpreted as a rough approximation of a heart. We simulate the imaging of a one-head SPECT by computing 60 angularly equidistant projections with 64×64 pixels each. To this end, we construct a projection matrix which contains the probabilities that at a specific detector position a photon emitted in a specific voxel. From this, an image may be created by interpreting the value of an image voxel as the mean activity in that voxel. To keep the issue of interest clear, we do not simulate noise, scatter or absorption. To evaluate the quality of the obtained reconstruction we employ the commonly used measure

$$\text{err} = \frac{\sum_i |\text{recon}_i - \text{original}_i|}{\#\text{counts}} * 100\% \tag{5}$$

Motion time	Projection	Motion time	Projections
1	15	4	10, 41
2	30	5	30, 42
3	41	6	5, 51
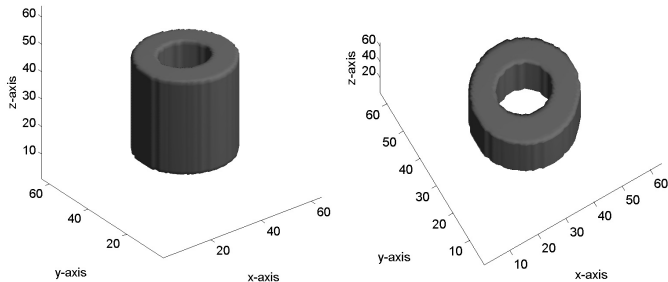
Fig. 1. An academic $64 \times 64 \times 64$ image.

over all voxels i with #counts $= \sum_i \text{original}_i$. Table I shows four different types of motion which were used in our experiments. The rotation and translation parameters were chosen such that every parameter is used at least in one test, and such that a reconstruction without motion correction would be distorted by motion artifacts. The rotation angle α, β and γ are measured in degree whereas the translations t_x, t_y and t_z are measured in voxel. Hear α is a rotation around the z-axis, β around the x-axis, and γ around the y-axis (see figure 2). The z-axis corresponds to the axis of rotation of the camera heads, and the rotation was approximately about the center of rotation of the camera heads, which corresponds to the center of the test image (here $c_{rot} = (32, 32, 32)^\top$)
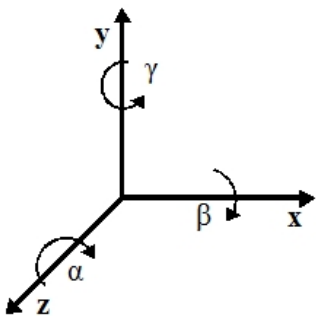
Fig. 2. Used coordinate system where the z-axis corresponds to the axis of rotation of the camera heads.

TABLE I

MOTION PARAMETER.

Motion parameter	α	β	γ	t_x	t_y	t_z
1	5.0	-6.0	3.0	0.0	0.0	0.0
2	0.0	7.0	0.0	-4.3	5.2	-3.4
3	5.0	3.0	-9.0	1.2	-1.1	5.0
4	-5.0	0.0	6.0	0.0	4.2	-3.9

Next, we list in table II the projection number after which a motion occurred. Here we designed altogether six experiments, three of which consist of one movement (1,2,3) and two movements (4,5,6), respectively.

We start out by applying an EM reconstruction without motion correction, an OSEM reconstruction incorporating the DDMC scheme, and our new EMMC and OSEMMC reconstructions to the set ups with one movement and all four

motion parameter sets, ending up in twelve test scenarios. For OSEM, EMMC, and OSEMMC we assumed that the motion parameters are known.

For the OSEMMC reconstruction we have chosen the projection subsets $\{1, 4, \cdots, 55, 58\}$, $\{2, 5, \cdots, 56, 59\}$, and $\{3, 6, \cdots, 57, 60\}$. The idea was to incorporate a better part of all projections in each subset. An interesting paper concerning the clever choice of subsets is [21]. Note, there is no correlation between the movement time and the chosen subsets. For the OSEM scheme we employed the two subsets defined by the motion states (see table II). We stopped the EM and EMMC schemes after 24 steps, whereas the OSEM scheme used 12 (2 subsets) and the OSEMMC scheme 8 steps (3 subsets), respectively. The iteration counts are chosen such that the respective execution times of the various schemes are comparable. Table III displays the obtained reconstruction error (5) for all test runs. These numbers are to be compared to a reconstruction error of 9.65% for the EM algorithm with 24 iteration-steps, when applied to the motion-free academic test image. As it is apparent, both the EMMC and OSEMMC scheme are close to the motion-free result and are superior to the original OSEM scheme. Also, a visual inspection of all motion corrected test cases shows meaningful results, demonstrated by two representative examples in Figure 3. One should note that we expected this result, due to the fact that the original OSEM scheme was not designed for the used SPECT system. In case of a dual head SPECT system with perpendicular heads we await similar results for EMMC, OSEMMC, and the original OSEM scheme. Next, we apply all four schemes to the test scenario with two motions. The same three subsets were again used for the OSEMMC approach and the subsets for OSEM were given by the three different motion states (see table II). Both schemes were stopped after 8 iteration steps (3 subsets), whereas the EM and EMMC were again stopped 24 steps. Table IV shows the improvement in the reconstruction error by including the motion information in the reconstruction. Once more, the EMMC and OSEMMC show an impressive behavior when compared to the motion-free reconstruction error of 9.65%. Again, a visual inspection of the results in Figure 4 does show promising results for the motion corrected schemes.

B. Phantom experiment

In this section we report on experiments with the Benchmark-Jaszczak-Phantom. The 120 projections were recorded using a dual headed gamma-camera-system of the MiE company (Seth, Germany). The image size was $128 \times 128 \times 128$ voxels after reconstruction. To mimic patient movement, the phantom was attached to a robot arm which allows for a user prescribed precise rigid motion. For comparison the

TABLE III

RECONSTRUCTION ERROR FOR THE EXPERIMENTS WITH ONE MOVEMENT. HERE, i ENCODES THE CORRESPONDING MOTION TIME AND j THE ASSOCIATED MOTION PARAMETERS. FROM TOP TO BOTTOM THE ROWS LIST THE ERROR FOR AN EM RECONSTRUCTION WITHOUT MOTION CORRECTION, A OSEM RECONSTRUCTION USING THE DDMC SCHEME, AND OUR NEW EMMC AND OSEMMC RECONSTRUCTION ALGORITHMS.

i,j	1, 1	1, 2	1, 3	1, 4	2, 1	2, 2	2, 3	2, 4	3, 1	3, 2	3, 3	3, 4
EM	19.44	95.62	47.01	62.40	16.12	57.54	32.23	42.28	13.71	47.43	24.85	29.60
OSEM	13.22	13.19	13.15	13.31	10.35	10.37	10.32	10.36	12.67	12.68	12.63	12.81
EMMC	10.72	10.69	10.69	10.79	10.15	10.16	10.12	10.17	10.00	10.01	9.97	10.13
OSEMMC	10.71	10.69	10.68	10.78	10.15	10.15	10.12	10.17	10.00	10.00	9.97	10.12

original	motion EM	OSEM	EMMC	OSEMMC
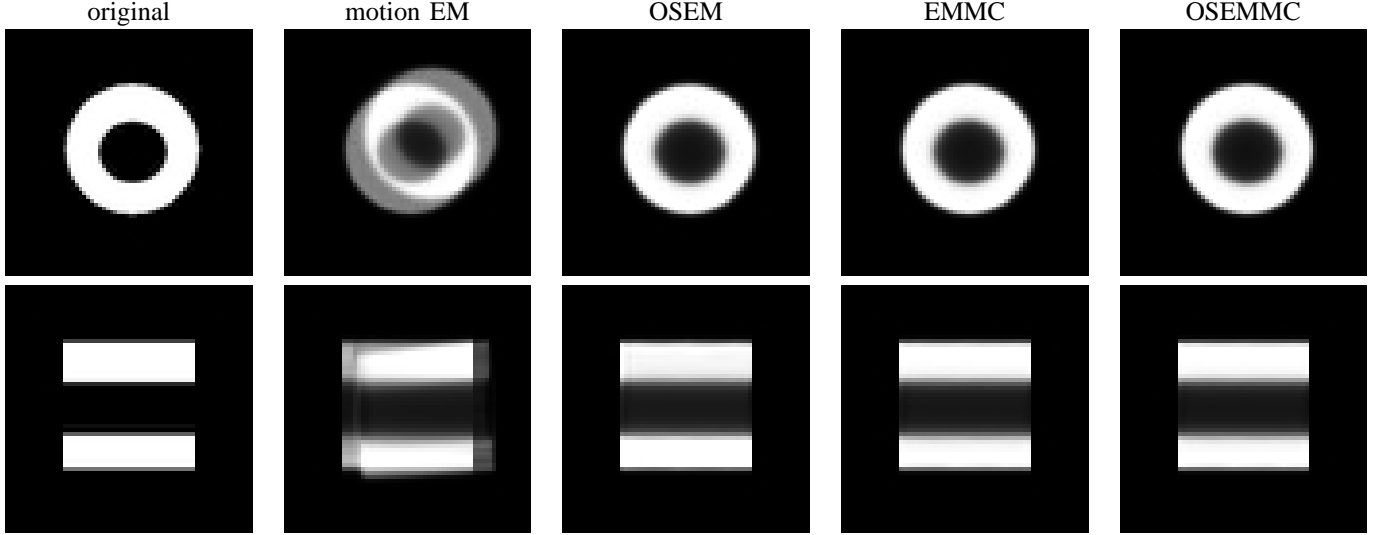
Fig. 3.   Representative slices, top row: test 2, 2 and slice 28 in the x-y-plain; bottom row: test 3, 3 and slice 29 in the x-z-plain. From left to right we present the original phantom, an EM reconstruction without motion correction, an OSEM reconstruction using the DDMC scheme, and results for the new EMMC and OSEMMC reconstructions.

phantom was also imaged without any motion. We performed a number of experiments. Here, we report on one representative experiment. The phantom was moved twice around the z-axis, which corresponds to the height of the cylinder and coincides approximately with the center of rotation of the dual heads. At projection 53 the phantom was rotated by $7°$ and by $-6°$ at projection 91. To validate the results, we compare (see Figure 5) the motion-free reconstruction with the results of our various schemes. The EM and EMMC run for 30 iteration steps. OSEM using the DDMC scheme as well as OSEMMC were stopped after 10 steps, each using three subsets. The

OSEM was based on the subsets $\{1, ..., 53\}$, $\{54, ..., 91\}$, and $\{92, ..., 120\}$, defined by the three different motion states described above. The OSEMMC was based on the projection subsets $\{1, 4, \cdots, 115, 118\}$, $\{2, 5, \cdots, 116, 119\}$ and $\{3, 6, \cdots, 117, 120\}$, to demonstrate that the choice of subsets may not necessarily be connected to the motion states in our new scheme. As it is apparent, OSEMMC again does produce satisfactory results. In particular it is superior to OSEM, due to the used SPECT system. The pipes and spheres of the phantom are sharper as compared to the motion corrupted reconstruction. But using a dual head SPECT system

TABLE IV

RECONSTRUCTION ERROR FOR THE EXPERIMENTS WITH TWO MOVEMENT. HERE, i ENCODES THE CORRESPONDING MOTION TIMES AND j AND k THE ASSOCIATED MOTION PARAMETERS. FROM UP TO DOWN THE ROWS LIST THE ERROR FOR AN EM RECONSTRUCTION WITHOUT MOTION CORRECTION, A OSEM RECONSTRUCTION USING THE DDMC SCHEME, AND OUR NEW EMMC AND OSEMMC RECONSTRUCTION ALGORITHMS.

i,j,k	4, 1, 2	4, 1, 3	4, 1, 4	4, 2, 3	4, 2, 4	4, 3, 4	5, 1, 2	5, 1, 3	5, 1, 4
EM	54.35	31.90	36.76	72.14	79.95	51.50	49.97	27.69	32.25
OSEM	13.40	13.37	13.50	13.43	13.54	13.49	12.94	12.80	13.09
EMMC	10.80	10.77	10.94	10.79	11.10	10.90	10.28	10.12	10.46
OSEMMC	10.80	10.77	10.94	10.79	10.95	10.90	10.27	10.12	10.45
i,j,k	5, 2, 3	5, 2, 4	5, 3, 4	6, 1, 2	6, 1, 3	6, 1, 4	6, 2, 3	6, 2, 4	6, 3, 4
EM	35.54	39.47	36.62	45.65	29.56	36.04	87.53	93.43	58.77
OSEM	12.81	12.89	13.12	17.04	16.87	17.36	16.74	17.11	17.29
EMMC	10.13	10.28	10.47	11.17	11.05	11.29	11.06	11.50	11.24
OSEMMC	10.12	10.27	10.46	11.19	11.04	11.27	11.05	11.22	11.22
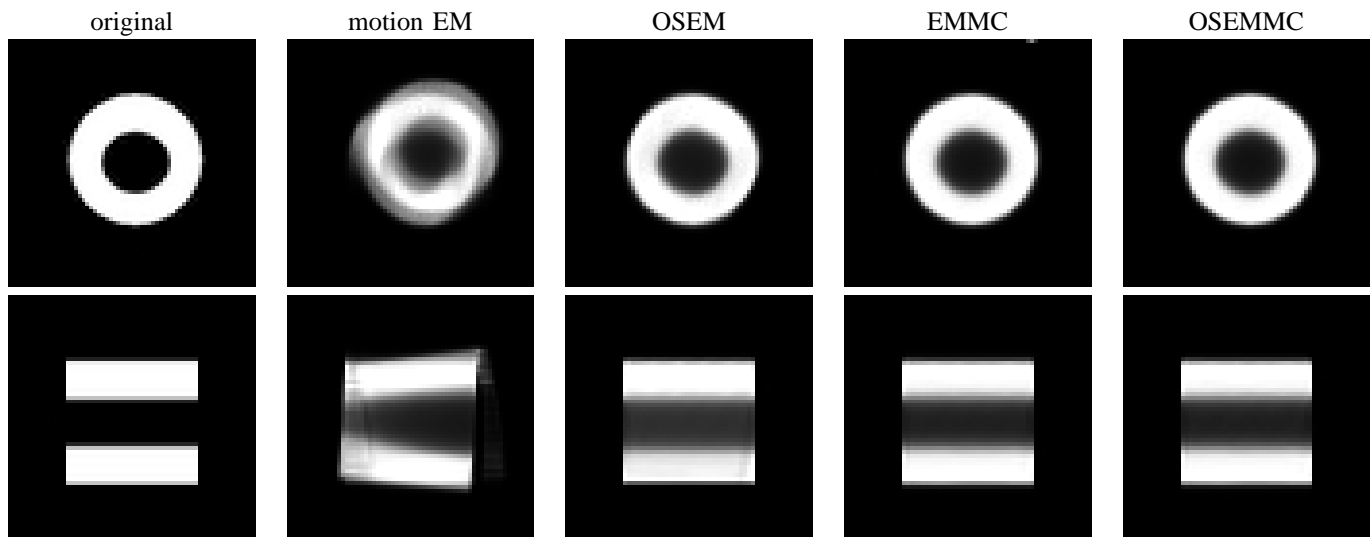
Fig. 4. Representative slices, top row: test 4, 2, 4 and slice 23 in the x-y-plain; bottom row: test 6, 1, 3 and slice 38 in the y-z-plain. From left to right we present the original phantom, an EM reconstruction without motion correction, an OSEM reconstruction using the DDMC scheme, and results for the new EMMC and OSEMMC reconstructions.
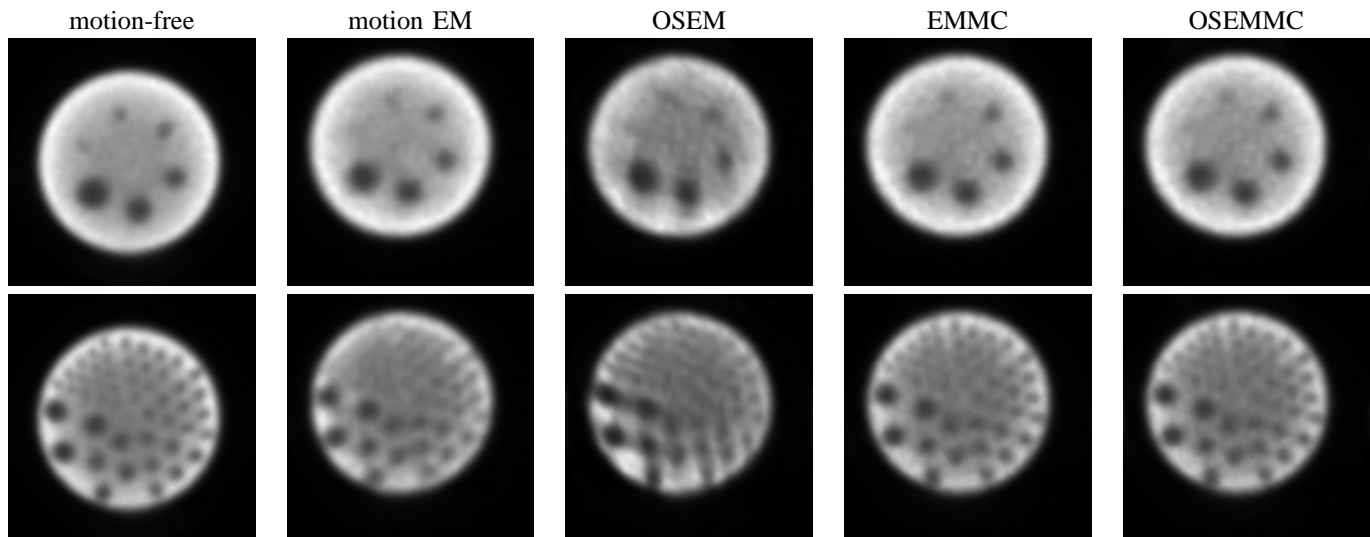
Fig. 5. Representative slices. Top row: slice 36; bottom row: slice 68. From left to right we present the original phantom, an EM reconstruction without motion correction, an OSEM reconstruction using the DDMC scheme, and results for the new EMMC and OSEMMC reconstructions.

with perpendicular heads we expect similar results from all three schemes. However, the motion-free reconstruction is still somewhat sharper which is on account of the interpolation artifacts within the projection/backprojection scheme.

IV. DISCUSSION

We developed and validated a new flexible framework for the incorporation of motion information in the projector/backprojector pair of a reconstruction algorithm to facilitate compensation for rigid-body motion which overcomes a restriction of the DDMC reconstruction scheme. Unlike other schemes, the new framework allows for the incorporation of user prescribed projection independent of the used camera system and/or the actual motion states in the measured data. We implemented the new methodology for the well-known

EM and OSEM schemes and validated its performance for both an academic example and real phantom images. The preliminary test results turned out to be very promising as the new schemes consistently overcome a restriction of the conventional approaches. However, we still have to assume that the motion parameters are known beforehand. We are currently working on schemes which combine both motion estimation and reconstruction. Furthermore, the described reconstruction approach is, in its present state, restricted to motion occurring between the measured projections.

REFERENCES

[1] J. M. Wheat and G. M. Currie, "Incidence and characterization of patient motion in myocardial perfusion SPECT: Part 1," *J Nucl Med Technol*, vol. 32, no. 2, pp. 60–65, 2004.

[2] E. H. Botvinick, Y. Y. Zhu, W. J. O'Connell, and M. W. Dae, "A quantitative assessment of patient motion and its effect on myocardial perfusion SPECT images," *J Nucl Med*, vol. 34, no. 2, pp. 303–310, 1993.

[3] J. A. Cooper, P. H. Neumann, and B. K. McCandless, "Effect of patient motion on tomographic myocardial perfusion imaging," *J Nucl Med*, vol. 33, no. 8, pp. 1566–1571, 1992.

[4] J. Friedman, K. Van Train, J. Maddahi, A. Rozanski, F. Prigent, J. Bietendorf, A. Waxman, and D. S. Berman, ""upward creep" of the heart: A frequent source of false-positive reversible defects during thallium-201 stress-redistribution SPECT," *J Nucl Med*, vol. 30, no. 10, pp. 1718–1722, 1989.

[5] C. Pellot-Barakat, M. Ivanovic, D. A. Weber, A. Herment, and D. K. Shelton, "Motion detection in triple scan SPECT imaging," *IEEE Trans Nucl Sci*, vol. 45, no. 4, pp. 2238–2244, 1998.

[6] A. M. Passalaqua and R. Narayanaswamy, "Patient motion correction of SPECT images: dual scan approach," *IEEE Proc. NSSS'94, Norfolk, VA*, vol. 3, pp. 1270–1274, 1995.

[7] K. J. Lee and D. C. Barber, "Use of forward projection to correct patient motion during SPECT imaging," *Phys Med Biol*, vol. 43, pp. 171–187, 1998.

[8] Q.-s. Chen, P. R. Franken, M. Defrise, M. H. Jonckheer, and F. Deconinck, "Detection and correction of patient motion in SPECT imaging," *J Nucl Med Technol*, vol. 21, no. 4, pp. 198–205, 1993.

[9] M. Oghabian, I. Mohammadi, S. Sarkar, and A. Karimian, "Motion correction of SPECT projection before reconstruction," *12th International Conference in Central Europe on Computer graphics, Visualization and Computer vision*, 2003.

[10] R. R. Fulton, S. Eberl, S. R. Meikle, B. F. Hutton, and M. Braun, "A practical 3D tomographic method for correcting patient head motion in clinical SPECT," *IEEE Trans Nucl Sci*, vol. 46, no. 3, pp. 667–672, 1999.

[11] A. Z. Kyme, B. F. Hutton, R. L. Hatton, D. W. Skerrett, and L. R. Barnden, "Practical aspects of a data-driven motion correction approach for brain SPECT," *IEEE Trans Med Imag*, vol. 22, no. 6, pp. 722–729, 2003.

[12] R. Fulton and S. Meikle, "Reconstruction of projection data corrupted by rigid or non-rigid motion," in *Conference Record of the 2005 IEEE Nuclear Science Symposium and Medical Imaging Conference, San Juan*, 2005.

[13] E. Röhl, H. Schumacher, and B. Fischer, "Automatic detection of abrupt patient motion in spect data acquisition," in *Proceedings of SPIE, Medical Imaging, Image Processing*, 2007.

[14] B. Feng, H. C. Gifford, R. D. Beach, G. Boening, M. A. Gennert, and M. A. King, "Use of the three-dimensional gaussian interpolation in the projector/backprojector pair for compensation of the known rigid-body motion in SPECT," *IEEE Transactions on Medical Imaging*, vol. 25, pp. 838–844, 2006.

[15] H. M. Hudson and R. S. Larkin, "Accelerated image reconstruction using ordered subsets of projection data," *IEEE Trans Med Imag*, vol. 13, no. 4, pp. 601–609, 1994.

[16] L. A. Shepp and Y. Vardi, "Maximum likelihood reconstruction for emission tomography," *IEEE Trans Med Imag*, vol. MI-1, pp. 113–122, 1982.

[17] M. I. Miller, D. L. Snyder, and T. R. Miller, "Maximum-likelihood reconstruction for single-photon emission computed-tomography," *Trans Nuc Sci*, vol. NS-32, no. 1, pp. 769–778, 1985.

[18] P. Schmidlin, M. E. Bellemann, and G. Brix, "Iterative reconstruction of PET images using a high-overrelaxation single projection algorithm," *Phys Med Biol*, vol. 42, pp. 569–582, 1997.

[19] P. Bruyant, "Analytic and iterative reconstruction algorithms in SPECT," *J Nucl Med*, vol. 43, no. 10, pp. 1343–1358, 2002.

[20] G. H. Golub and C. F. Van Loan, *Matrix-computations*. Oxford : North Oxford Academic, 1983.

[21] S. R. Meikle, B. F. Hutton, D. L. Bailey, P. K. Hooper, and M. J. Fulham, "Acceleration EM reconstruction in total-body PET: potential for improving tumour detectability," *Phys. Med. Biol.*, vol. 39, pp. 1689–1704, 1994.